Journal of Building Engineering 82 (2024) 108169

Contents lists available at ScienceDirect

Journal of Building Engineering

journal homepage: www.elsevier.com/locate/jobe

Applicability of a dedicated outdoor air system assisted by isothermal dehumidification and evaporative cooling

Seong-Yong Cheon [a], Hye-Jin Cho [b], Jae-Weon Jeong [a,*]

[a] Department of Architectural Engineering, College of Engineering, Hanyang University, Seoul, Republic of Korea
[b] Sustainable Urban Systems Center, Hanyang Institute for Energy and the Environment, Seoul, Republic of Korea

ARTICLE INFO

Keywords:
Isothermal dehumidifier
Indirect evaporative cooler
Dedicated outdoor air system
Energy simulation

ABSTRACT

A dedicated outdoor air system (DOAS) assisted by an isothermal dehumidifier and an indirect evaporative cooler is proposed, and its energy-saving potential is evaluated based on detailed simulations. In the proposed system, an isothermal dehumidifier accommodates the latent cooling load and an indirect evaporative cooler assumes a sensible cooling load. The energy performance of the proposed system was evaluated by comparing it with two conventional dedicated outdoor air systems: a DOAS with a desiccant wheel and a DOAS with a cooling coil. The results indicate that the proposed DOAS can accommodate sensible and latent cooling loads, but it consumes 10% more operating energy because of the low coefficient of performance (COP) (0.67) of the isothermal dehumidifier, despite the free cooling operation by the indirect evaporative cooler. For comparable energy performance, the proposed system requires the COP of the isothermal dehumidifier to be greater than 0.78, which is achieved through improvements in the membrane selectivity and vacuum pump (compression ratio and isentropic efficiency).

Nomenclature

A	Area [m^2]
C	Heat capacity [J/°C]
c_p	Specific heat capacity [kJ/kg·°C]
DHR	Difference of humidity ratio [−]
g	Gravitational acceleration [m/s^2]
h	Enthalpy [kJ/kg]
h_{fg}	Latent heat of water evaporation [kJ/kg]
k	Diffusion velocity [m/s]
M	Molar mass [kg/mol]
$\dot{m}$	Mass flow rate [kg/s]
$\dot{n}$	Molar mass flow rate [mol/s]
N	Rotation speed of the desiccant wheel [rph]
NTU_m	Number-of-mass-transfer unit [−]
P	Power [W]

* Corresponding author.
E-mail address: jjwarc@hanyang.ac.kr (J.-W. Jeong).

https://doi.org/10.1016/j.jobe.2023.108169
Received 7 August 2023; Received in revised form 31 October 2023; Accepted 14 November 2023
Available online 21 November 2023

p	Pressure [Pa]
Per	Permeance [mol/(m^2 · s · Pa)]
$\dot{Q}$	Heat capacity [kW]
R	Ideal gas constant [m^3 · Pa/(K · mol)]
RH	Relative humidity [%]
S	Selectivity [−]
T	Temperature [°C]
U	Overall heat transfer coefficient [W/(m^2 · °C)]
V	Air velocity [m/s]

Greek Symbols

γ	Adiabatic expansion coefficient [−]
Δ	Difference [−]
ε	Effectiveness [−]
η	Efficiency [−]
ω	Humidity ratio [kg/kg_a]

Subscripts

a	Air
c	Cooling
cc	Cooling coil
cws	Cooling water supply
d	Dry air
deh	Dehumidification
cap	Capacity
EA	Exhaust air
hc	Heating coil
i	Inlet
isen	Isentropic
lat	Latent
max	Maximum
mem	Membrane
min	Minimum
OA	Outdoor air
o	Outlet
pro	Process
RA	Return air
ref	Reference
reg	Regeneration
req	Require
SA	Supply air
sen	Sensible
sec	Secondary air
tar	Target point
tot	Total
v	Water vapor
vac	Vacuum
w	Water
zone	Conditioned zone

Abbreviations

CAPFT	Capacity as a function of temperature
COP	Coefficient of performance
DOAS	Dedicated outdoor air system
DW	Desiccant wheel
EIRFPLR	Electric input to cooling output factor
EIRFT	Energy input ratio as a function of temperature
PLR	Part load ratio
SLHR	Sensible to latent heat ratio
ID	Isothermal dehumidifier
IEC	Indirect evaporative cooler

1. Introduction

The building sector is one of the largest energy consumers, accounting for 35% of the global total energy. The International Energy Agency (IEA) reported a technological roadmap for the building sector to achieve energy savings while avoiding expected energy increases [1]. The roadmap leads to buildings using highly insulated external walls and thermally improved windows, which reduce the sensible heat transfer from the external environment through building envelopes. As the energy performance of building envelopes improves, the sensible cooling loads of buildings decrease, the moisture generated as an internal heat gain from occupants and activities remains unchanged. This can lead to cooling loads of buildings with a higher fraction of latent loads than typical buildings, which causes indoor occupant discomfort at high humidity levels [2,3].

In energy-efficient buildings, air-conditioning systems using cooling coils for dehumidification [4] reduce the cooling setpoint to control indoor humidity; however, a vapor compression refrigeration system (VCS), which is the most commonly used for heating, ventilation, and air-conditioning (HVAC) applications, dehumidifies air by condensation dehumidification. The moisture from the air condenses on a cold surface below the dew point temperature of entering air, and then the dehumidified air should be reheated before supplied to indoors for avoiding over-cooled environments. Additionally, the condensate water would lead to breeding environment for Legionella and other airborne bacteria [5,6]. To address these challenges, desiccant materials (i.e., active desiccant wheels (DWs) and liquid desiccants) based air conditioning system have been suggested as an alternative to the traditional dehumidification method [7,8]. These systems remove moisture from the air through the process of absorption/adsorption and regeneration using the vapor pressure of the desiccant and the vapor pressure of the air. To maintain dehumidification performance, the desiccant based dehumidification systems requires regeneration heating source (i.e., 60–90 °C), and it would consume substantial amount of the heating energy if the renewable energy (i.e., solar energy) or other low grades heat source is not provided [9–16].

Isothermal dehumidifiers (IDs) using membranes have emerged as promising technologies and are comparable to and more thermodynamically efficient than conventional dehumidification systems in that they dehumidify air through an isothermal process [17–24]. IDs dehumidify air through the pressure gradient of water vapor using a vacuum pump. The membranes for active dehumidification systems are dense and fabricated from polymeric materials with high selectivity and permeability to water vapor [17,18]. The dehumidification process performed by an ID involves mass transfer through diffusion. The air is dried without a change in temperature, and no heating or cooling source is used for dehumidification. In addition, the ID system can avoid bio-contamination during the dehumidification process because condensation water is not generated in the system.

In Reference [19], the dehumidification performance (i.e., water vapor removal and coefficient of performance (COP)) of an isothermal dehumidifier was evaluated by considering the following parameters: velocity and humidity of the feed air, permeance and selectivity of the membrane for water vapor, and vacuum pressure. The selectivity of the membrane and vacuum pressure had the greatest influence on the dehumidification performance, with a trade-off between water vapor removal and the COP. Bui et al. [20] analyzed the energy performance of an isothermal dehumidifier using the COP under various air conditions and membrane properties. The results indicated that the COP of the isothermal dehumidifier can theoretically be 2–3 when a vacuum operates in an isentropic compression state.

In previous studies [21–23], advanced system configurations using membranes for IDs were proposed to improve dehumidification and energy performance. Scovazzo et al. [21,22] proposed an ID using a sweep gas operation method that uses a portion of the process air dehumidified by a membrane and supplied to the permeate side to enhance the vapor pressure gradient. Experimental results indicated that the sweep gas dehumidification system can achieve a dehumidification efficiency of more than 200% of that of a conventional dehumidification system. Claridge et al. [23] proposed a Claridge–Culp–Liu dehumidifier, which is an ID that uses a cooling coil; it is installed downstream of a vacuum pump, and it reduces the discharge pressure of the vacuum pump to reduce the vacuum compression ratio. The results indicated that the proposed system can save 26% of the operating energy compared with conventional vapor compression systems under ideal conditions.

Several studies have shown the dependence of the dehumidification performance on the membrane material, membrane shape (e.g., flat sheet and hollow fiber), and system configuration (e.g., sweep gas type); however, only a few relevant studies on utilizing IDs in building applications have been conducted. In this paper, we propose a system using an ID and an indirect evaporative cooler (IEC) in a dedicated outdoor air system (DOAS) for the adjustment of latent and sensible cooling, respectively, which fully operates with thermally decoupled sensible and latent heat using an ID; the IEC can improve its energy performance using free cooling. The energy

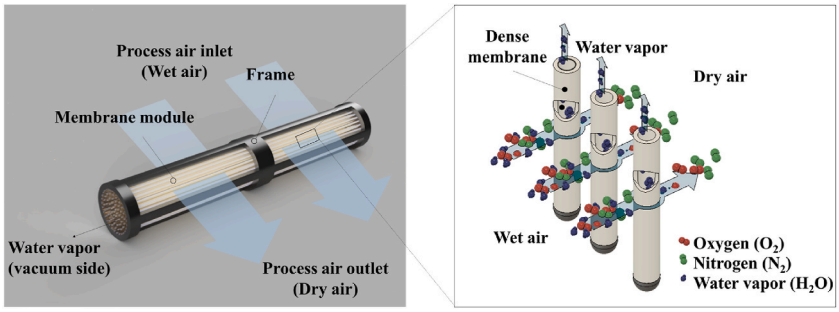

Fig. 1. Isothermal dehumidifier (ID) and dehumidification process.

performance of the proposed system was evaluated through detailed energy simulations using models and was compared with conventional systems. To evaluate the energy performance under various conditions, we conducted a parametric study using independent variables that affect the energy performance of the proposed system to enhance the system COP.

2. System overview

2.1. Proposed DOAS

The ID used in the proposed DOAS to manage the latent load of a building consists of membrane modules and a vacuum pump. The ID and membrane modules (Fig. 1) are bundles of hollow fiber membranes with dense membrane characteristics for gas separation. A dense membrane separates moisture from wet air through a partial vapor pressure gradient. When the process air is supplied to the membrane module (i.e., the outer side of the hollow fiber), the water vapor in the process air permeates through the hollow-fiber membranes owing to the pressure gradient to the permeate side (i.e., the inner side of the hollow fiber) under vacuum pumping.

The water vapor from the moist air flowing through the process air is absorbed by the membrane, and the absorbed water vapor diffuses through the membrane and desorbs to the permeate side. Water vapor permeating the wet air is discharged to the exhaust side of the vacuum pump. The ID performs isothermal dehumidification under a pressure gradient using the vacuum pump, and the water vapor in the process air permeates the membrane without changing the air temperature.

As shown in Fig. 2, the proposed DOAS (ID-IECDOAS) consists of an ID and IEC. As shown in Fig. 2a and A.1, the ID consists of membrane modules and vacuum compressors, and the IEC consists of a heat-exchanger core and a water distributor for evaporation. The DOAS supplies minimum ventilation with dehumidified air to manage the latent load of the conditioned zones, providing supply air (SA) at a neutral temperature. The remaining sensible load in the zones is managed using mechanical cooling and heating devices (e.g., fan coil unit, radiant cooling panel, and heat pump).

The proposed DOAS manages latent and sensible cooling as thermally decoupled processes using the ID and IEC, respectively. In typical operation, when outdoor air (OA) is hot and humid, the introduced air is dehumidified using the ID to satisfy the target humidity ratio. Subsequently, when the temperature of the dry air passing through the ID is higher than the room air (RA) temperature, the IEC is activated with a wet operation, which uses the free cooling of evaporation to spray water to the exhaust air stream (i.e., the secondary air of the IEC) to satisfy the SA temperature (e.g., 24 °C in summer). If the SA temperature decreases below the neutral temperature, causing overcooling in the conditioned zone, the IEC can activate the dry-cooling mode, functioning as a heat exchanger from the SA to the exhaust air stream, or it can deactivate to a bypass operation.

Considering the thermodynamic characteristics of the proposed system, we propose a detailed operation mode controlled by the outdoor and indoor air conditions in four regions: hot and humid air (region 1), cool and humid air (region 2), hot and dry air (region 3), and cold and dry air (region 4). As shown in the psychrometric chart of the OA (Fig. 3), the operating region of the proposed system is classified based on the target humidity ratio and temperature of the RA. The humidity ratio of the introduced air determines the operation of the ID using the target humidity ratio, whereas the air temperature determines the IEC operation (e.g., wet, dry, and bypass modes).

In mode 1, when the humidity ratio and temperature of the OA are higher than those of the RA, the ID dehumidifies the introduced air to satisfy the target humidity (i.e., 7.63 g/kg). The IEC then activates the wet operation to passively cool the process air to satisfy the target temperature (i.e., 24 °C). Fig. 4 a shows the thermal processes of the air streams (process air and exhaust air) in mode 1 using

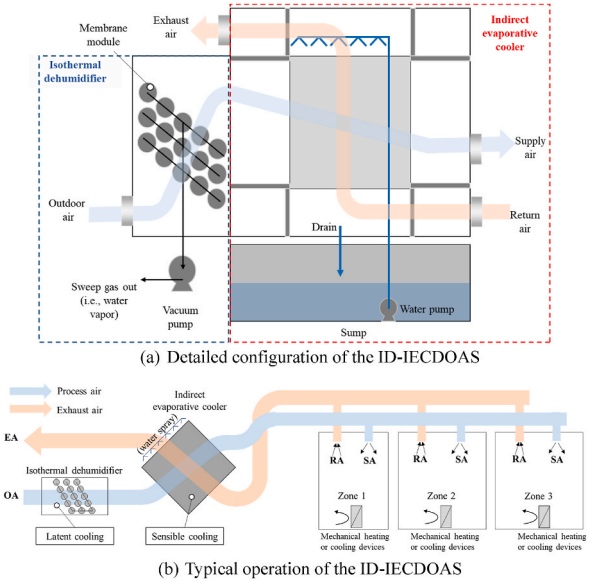

Fig. 2. Schematic and typical operation of the ID-IECDOAS (a) Detailed configuration of the ID-IECDOAS (b) Typical operation of the ID-IECDOAS.

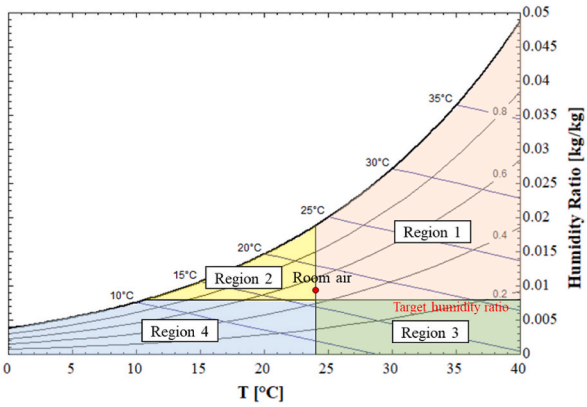

Fig. 3. Operation regions of the psychrometric chart.

psychrometric charts.

As Fig. 4 b shows, if the temperature of the OA is lower than that of the RA, and the humidity ratio of the OA is higher than the target humidity ratio of the SA, the proposed DOAS operates in mode 2. In region 2, the ID dries the process air to satisfy the target humidity ratio, and the IEC operates under room conditions in two modes: bypass and dry. In the bypass mode, the IEC is deactivated, air dehumidified by the ID is supplied to the conditioned zone, and the demand for a cooling load for a parallel system is alleviated by supplying the temperature of the process air (i.e., 17 °C) below the RA temperature. However, when the zone is under overcooling conditions or requires heating, the IEC is operated in the dry mode, which recovers sensible heat from the exhaust air and deactivates the water spray (Fig. 4c).

When the humidity ratio of the introduced OA is below the target value and the temperature was higher than the RA temperature, as shown in region 3, there is no demand to dry the process air, and the ID is deactivated (or bypassed) to avoid unnecessary dehumidification. When the temperature of the introduced air that bypasses the ID is higher than the neutral temperature, the IEC performs a wet operation via evaporative cooling. Otherwise, the temperature of the introduced air is lower than the neutral temperature (region 4), and the IEC performs a dry operation by recovering heat from the exhaust air stream. Fig. 4d shows the sequence for each operation region of the proposed system under various air conditions.

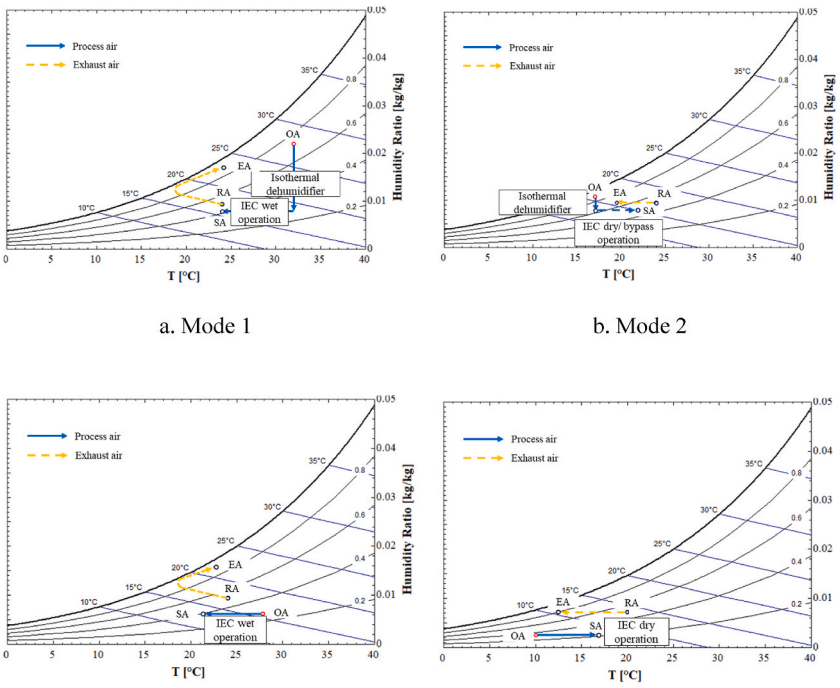

Fig. 4. Operation modes of the ID-IECDOAS a. Mode 1 b. Mode 2 c. Mode 3 d. Mode 4.

2.2. DW-DOAS

The DW-DOAS is a conventional DOAS that uses a DW for dehumidification. As shown in Fig. 5, the DW-DOAS consists of an active DW, regeneration heater, heat exchanger, and cooling coil. The DW-DOAS has three different modes based on the introduced OA conditions: humid air, hot and dry air, and cold and dry air.

Under humid air conditions (Fig. 6a and b), when the humidity ratio of the OA is higher than the target value, the active DW dehumidifies the introduced air to satisfy the target humidity ratio. The secondary air of the exhaust air stream passing through the heat exchanger is heated using a regeneration heating coil to regenerate the DW. The passage of dried air through the DW is almost isenthalpic; the temperature of the dehumidified air (e.g., 65 °C) is sufficiently high to supply to the conditioned zone. The process air passing through the DW is precooled using a heat exchanger with the exhaust of the RA. Finally, the cooling coil controls the SA temperature to satisfy the target temperature (i.e., neutral temperature) with a dry cooling operation.

When the OA is hot and dry, its intake, which is lower than the target humidity ratio, bypasses the DW. The heat exchanger is operated to precool the OA, and the air temperature is controlled using a cooling coil to satisfy the neutral temperature. When the OA is cold and dry, the DW is bypassed, similar to the hot and dry conditions. The heat exchanger is operated to recover heat from the exhaust air. If the air temperature passing through the heat exchanger is lower than the neutral temperature (i.e., 20 °C in winter), the heating coil is operated to satisfy the target temperature. The operation sequence for each air condition of the DW-DOAS is shown in Fig. 6.

2.3. CC-DOAS

Fig. 7 shows the CC-DOAS, which is a DOAS type that uses a cooling coil for dehumidification and consists of an enthalpy exchanger, cooling coil, and reheating coil. The operation of the CC-DOAS is classified into four modes based on the OA conditions: high enthalpy and humid air, low enthalpy and humid air, hot and dry air, and cold and dry air.

When the OA is under high-enthalpy and humid-air conditions (Fig. 8a), in which the enthalpy and humidity of the OA are higher than those of the RA and the target humidity ratio, the enthalpy exchanger precools and pre-dehumidifies the process air of the OA with the RA exhaust. Subsequently, the preconditioned air is fully dried using the cooling coil to satisfy the target humidity ratio with condensation at the saturation point (i.e., 10 °C and 100% relative humidity (RH)). When the temperature of the air passing through the cooling coil is lower than the target temperature, which can be in an over-cooling state to supply the conditions zone, the reheat coil is activated to satisfy the target temperature (i.e., 24 °C).

When the OA is under low-enthalpy and high-humidity conditions (Fig. 8b), the enthalpy exchanger is bypassed, the cooling coil is activated for dehumidification to the target humidity, and the reheat coil is operated to satisfy the target temperature.

If the OA is hot and dry (Fig. 8c), the enthalpy exchanger preconditions the intake of OA and the exhausting of the RA. The cooling coil is operated to satisfy the target temperature using a dry cooling operation. If the OA is cold or dry (Fig. 8 d), the intake OA recovers heat and moisture from the exhaust air through the enthalpy exchanger, and the air passage can be controlled using a heat coil to satisfy the target temperature if it is lower than the neutral temperature. The operation sequence of the CC-DOAS is shown in Fig. 8.

3. Simulation overview

A detailed energy simulation was conducted to estimate the energy performance of the studied DOASs. The load building (i.e., sensible and latent loads) was evaluated using the software TRNSYS. The minimum ventilation air flow rates for the DOASs were designed according to ASHRAE Standard 62.1 [24]. The outlet air conditions and energy consumption of each component were estimated using an equation-based simulation model and Engineering Equation Solver.

3.1. Model building

A simulation building model was created using TRNSYS 17 to estimate the hourly sensible and latent loads [25]. The building was assumed to be an office, with a floor area of 100 m^2 and a ceiling height of 3 m, and located in Seoul, Korea. The thermal properties of the building envelope were set according to the local standards of the energy-conservation building code [26,27], which describes a highly energy-efficient building that shares the criteria for a passive house. The U-values of the building envelope were determined to be 0.15 W/(m^2· °C) for the roof and 0.17 W/(m^2· °C) for the exterior walls. The windows were located to the south, and the window-to-wall area ratio was set to 0.17. Internal gains were determined for the occupants, lights, and a computer. The internal heat from the occupants was set to 75 W/person for sensible heat and 45 W/person for latent heat [28], and the lighting and computer generating sensible heat loads were set to 13 W/m and 140 W, respectively. The occupancy and heating, ventilation, and air

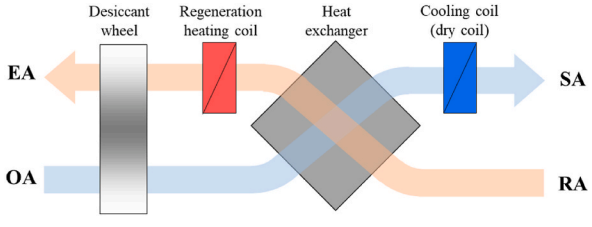

Fig. 5. Schematic of the DW-DOAS

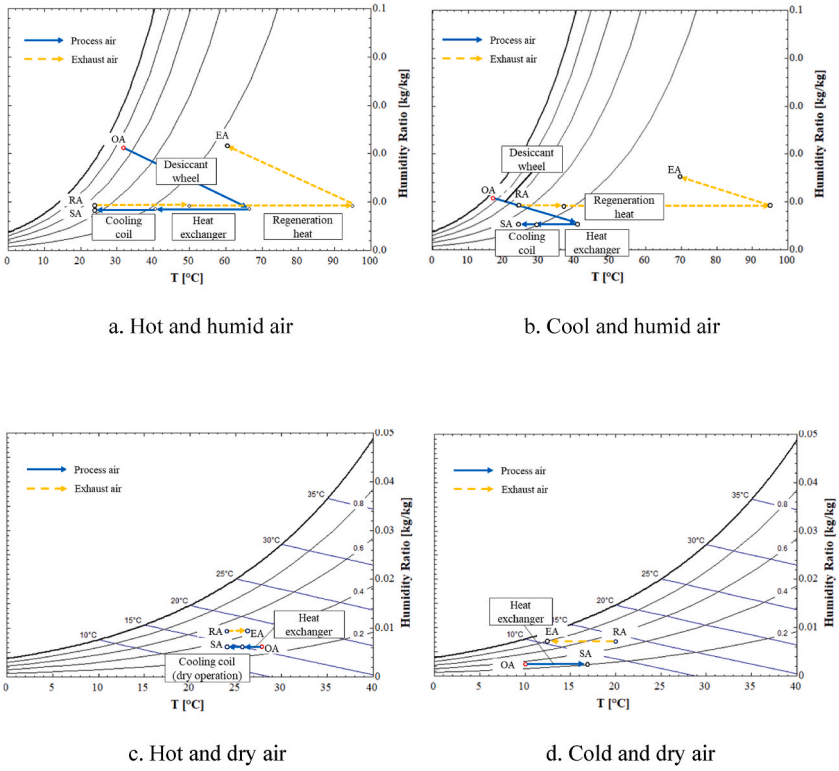

Fig. 6. Schematic and psychrometrics of the DW-DOAS a. Hot and humid air b. Cool and humid air c. Hot and dry air d. Cold and dry air.

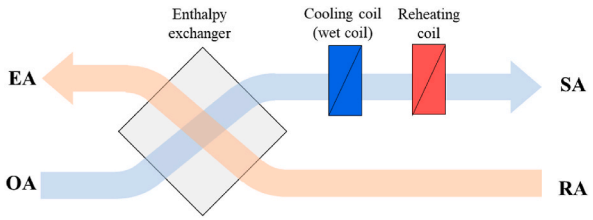

Fig. 7. Schematic and operation of the CC-DOAS in summer.

conditioning (HVAC) schedules were based on ASHRAE Standard 90.1 [29] for office buildings. The RA conditions were set to 24 °C and 50% RH during cooling and 20 °C and 50% RH during heating. The detailed settings of the physical parameters for the model-building simulation in the TRNSYS program are summarized in Table 1.

3.2. System component model

3.2.1. Isothermal dehumidifier

The ID dehumidifies the process air without a temperature change, and its energy is consumed by a vacuum pump to generate vacuum pressure and evacuate exhaust air. The conditions of the dried air passing through the ID were calculated using a simplified effectiveness–number-of-transfer unit (NTU) method [30,31], and the energy consumption of the vacuum pump was estimated using a compression work equation considering the isentropic efficiency [32].

A simplified effectiveness-NTU method was used to estimate the dehumidification performance of the ID in the proposed DOAS. As shown in Equation (1), the model consisting of the mass NTU (NTU_m) and X factor (X) evaluates the outlet humidity ratio passing the ID ($w_{pro,o}$). The mass NTU is defined as $kA\rho/\dot{m}$, which can be determined from the membrane properties (overall diffusion velocity of the membrane (k) and surface area of the membrane (A)) and air properties (density (ρ) and mass flow rate ($\dot{m}$)) [33,34]. The X factor is the ratio of the humidity difference of the process air to that on the permeate side (vacuum pump side). To avoid repetitive processes in determining the X factor for evaluating the outlet humidity ratio of the process air ($w_{pro,o}$), we simplified its value to the form of a mass NTU function, as shown in Equation (2).

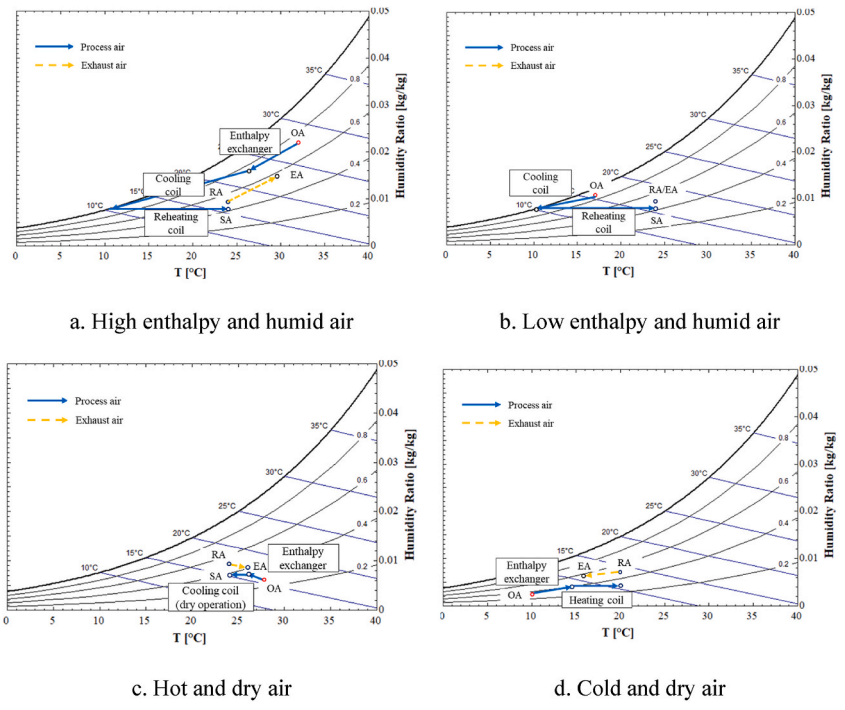

Fig. 8. Schematic and psychrometrics of the CC-DOAS a. High enthalpy and humid airb. Low enthalpy and humid air c. Hot and dry air d. Cold and dry air.

Table 1
Physical parameters of the model building.

Location	Seoul, Republic of Korea (IWEC2 weather data)	
Volume [m^3]	300 (10 × 10 × 3)	
U-value [W/(m^2· °C)]	Exterior wall	0.17
	Roof	0.15
	Window	1.3
Window-to-wall area ratio [−]	0.17	
Internal heat gain	People	5 persons
	Lights [W/ m^2]	13
	Computer [W]	700 (140 × 5)
Schedule	HVAC	ASHRAE Standard 90.1 (2013)
	Occupancy	ASHRAE Standard 90.1 (2013)
Room conditions	Cooling	24 °C and 50% RH
	Heating	20 °C and 50% RH

$$\varepsilon_{ID} = \frac{w_{pro,i} - w_{pro,o}}{w_{pro,i} - w_{per,i}} = \frac{1 - e^{-NTU_m(1-X)}}{1 - Xe^{-NTU_m(1-X)}}, \text{where} NTU_m = \frac{kA\rho}{\dot{m}} \text{ and } X = \frac{w_{per,i} - w_{per,o}}{w_{pro,i} - w_{pro,o}} \quad (1)$$

$$X_{simplified} = \frac{w_{per,o} - w_{per,i}}{w_{pro,i} - w_{per,i}} \frac{NTU_m}{1 + NTU_m} \quad (2)$$

The inlet humidity ratio of the permeate side (vacuum side) was estimated using a gray model that utilized mathematical equations and statistics (Equation (3)–(5)). In Equation (3), the inlet humidity ratio is determined by two factors: the outlet humidity ratio on the permeate side ($w_{per,o}$) and the difference in the humidity ratio (DHR) [31]. The outlet humidity ratio of the permeate side was defined using solution diffusion equations with two mixed gases (dry air and water vapor) rearranged into a quadratic equation (Equation (4)). The initial conditions consisted of the process air of the partial vapor pressures ($P_{pro,v,i}$ and $P_{pro,d.i}$), vacuum pressure of the permeate side (P_{vac}), and membrane properties for selectivity (S) to estimate the outlet humidity ratio of the permeate side. Equation (5) shows the polynomial-based regression model for the DHR, consisting of the NTU_m, vacuum pressure (P_{vac}), and membrane selectivity (S).

In this study, a polymer-based composite membrane was employed. We observed that the membrane dehumidification effectiveness was primarily determined by its permeance and selectivity. To estimate the dehumidification performance of the ID system, we set the separator conditions to GPU 680 with a selectivity of 50 and NTU 2 based on the experimental results of a previous study [36]. The physical properties of the membrane used for the ID design are summarized in Table 2. The model accuracy was evaluated

based on the simulated and measured outlet humidity ratio, and it was found that there was an error of within 15% (Appendix B).

$$w_{per,i} = (1 - \mathrm{DHR}) w_{per,o} \tag{3}$$

$$w_{per,o} = 0.62198 \frac{P_{vac}\frac{1}{1+R_{d,v}}}{P_{abm} - P_{vac}\frac{1}{1+R_{d,v}}}, \text{where} R_{d,v} = \frac{-SP_{pro,v,i} - SP_{vac} + P_{vac} - P_{pro,d.i} + \sqrt{\left(SP_{pro,v,i} - SP_{vac} + P_{vac} - P_{pro,d.i}\right)^2 + 4SP_{pro,v,i}P_{pro,d,i}}}{2SP_{pro,v,i}} \tag{4}$$

$$\begin{aligned}\mathrm{DHR} = {} & -0.07831 + 65.8574\frac{1}{S} + 0.02709\mathrm{NTU}_m + 0.02150\mathrm{P}_{vac} + 43.8420\frac{1}{s}\mathrm{NTU}_m - 8.27066\frac{1}{S}\mathrm{P}_{vac} \\ & - 0.01021\mathrm{NTU}_m\mathrm{P}_{vac} - 11540.6\frac{1}{S^2} + 0.01320\mathrm{NTU}_m^2 - 0.59997\frac{1}{S}\mathrm{NTU}_m\mathrm{P}_{vac} - 1846.65\frac{1}{S^2}\mathrm{NTU}_m + 620.975\frac{1}{S^2}\mathrm{P}_{vac} \\ & - 4.13216\frac{1}{S}\mathrm{NTU}_m^2 - 0.00036\mathrm{NTU}_m^2\mathrm{P}_{vac} + 649516\frac{1}{S^3} - 0.00110\mathrm{NTU}_m^3 + 68.0214\frac{1}{S^2}\mathrm{NTU}_m^2 \\ & + 23.3856\frac{1}{S^2}\mathrm{NTU}_m\mathrm{P}_{vac} + 32639.6\frac{1}{S^3}\mathrm{NTU}_m - 14641.3\frac{1}{S^3}\mathrm{P}_{vac} + 0.13925\frac{1}{S}\mathrm{NTU}_m^3 - 13083800\frac{1}{S^4} \\ & - 1.33680\frac{1}{S^2}\mathrm{NTU}_m^2\mathrm{P}_{vac} - 330.352\frac{1}{S^3}\mathrm{NTU}_m^2 - 127.998\frac{1}{S^3}\mathrm{NTU}_m\mathrm{P}_{vac} - 1.13280\frac{1}{S^2}\mathrm{NTU}_m^3 + 0.014896\frac{1}{S}\mathrm{NTU}_m^3\mathrm{P}_{vac} \\ & - 181956\frac{1}{S^4}\mathrm{NTU}_m + 91950.4\frac{1}{S^4}\mathrm{P}_{vac} + 76789100\frac{1}{S^5}\end{aligned} \tag{5}$$

The energy consumption of the vacuum pump in the proposed DOAS was estimated using the compression work of the vacuum pump, considering the isentropic pump work and isentropic efficiency (Equations (6) and (7)). The isentropic pump work was determined using the molar flow rate evacuated by the vacuum pump ($\dot{n}_{vac}$), air temperature (T_{kelvin}), compression ratio ($\frac{p_{amb}}{p_{vac}}$), ideal gas constant (R), and adiabatic expansion coefficient (γ), as shown in Equation (6). The ideal gas constant and adiabatic expansion coefficient were set to 8.31 J/(K·mol) and 1.4, respectively. The molar flow rate was determined by the air flow rate passing through the membrane layer, and the vacuum pressure was set to 1.0 kPa as the target vapor pressure, and 10 °C as the dew-point temperature for dehumidification as the design conditions of the DOAS. The isentropic efficiency of the vacuum pump was assumed to be 0.5, as reported in previous experimental studies [19,35].

$$\mathrm{P}_{vac,isen} = \dot{n}_{vac}\frac{\gamma R T_{kelvin}}{\gamma - 1}\left[\left(\frac{p_{amb}}{p_{vac}}\right)^{(\gamma-1)/\gamma} - 1\right] \tag{6}$$

$$\mathrm{P}_{vac} = \mathrm{P}_{vac,isen} / \eta_{vac,isen} \tag{7}$$

3.2.2. Indirect evaporative cooler

The IEC is a cooling system that maintains the target temperature without changing the humidity ratio through evaporation cooling and spraying water to the secondary air channel in wet operation modes (i.e., modes 1 and 3) [37]. In this study, the outlet temperature of the process air passing through the IEC was estimated using the wet-bulb effectiveness equation (Equation (8)). The wet-bulb effectiveness of the IEC is the ratio of the actual temperature difference to the maximum temperature difference between the dry-bulb temperature of the process air and the wet-bulb temperature of the secondary air (e.g., 17 °C wet-bulb temperature during cooling).

Based on previous studies [38,39], the wet-bulb effectiveness of the IEC in the wet mode was determined using the modified effectiveness-NTU method. The modified effectiveness-NTU method is an analytical model with the same equation as a general heat exchanger with a different Cr (the ratio of heat capacity) by considering the latent heat of vaporization of the secondary side, as shown in Equations (9) and (10): The modified Cr was calculated using the $\overline{K}$ factor (the ratio of the enthalpy difference to the wet-bulb temperature difference) considering the heat capacity ratio between the sensible and latent heat exchange on the secondary side. Generally, an HVAC system design for NTU ranges between 0.5 and 6 [40], and the range of $\overline{K}$ factors for IEC operation under the condition of no condensation on the process air side is between 3.25 and 3.55. To predict the air behavior characteristics of the process air condition, we assumed that the design NTU of the IEC was 2 and the $\overline{K}$ factor was 3.30.

Table 2
Physical properties of the membrane in the ID system.

Specifications	Values
Permeance ($\mathrm{Per_v}$)	680 GPU (2.08×10^{-7} mol/(m^2 · s · Pa)) [36]
Diffusion velocity of membrane (k)	5.18×10^{-4} m/s
Air flow rate to surface area of the membrane ($\dot{m}/A$)	1.82 (m^3/h)/m^2 [36]
Mass NTU (NTU_m)	2 (design conditions)
Effective selectivity (S)	50

* 1GPU = $3.35 \times 10^{-10} mol/(m^2 sPa)$.

$$\varepsilon_{IEC,wet} = \frac{T_{pro,i} - T_{pro,o}}{T_{pro,i} - T_{sec,i}^{wb}} \tag{8}$$

$$\varepsilon_{IEC,wet} = 1 - \exp\left[\left(\frac{NTU^{0.22}}{C_r}\left(\exp\left(-C_r NTU^{0.78}\right) - 1\right)\right], \text{where} C_r = C_{min}/C_{max}\right. \tag{9}$$

$$\begin{cases} C_{min} = \dot{m}_{pro} c_{pro,a} \\ C_{max} = \dot{m}_{sec}\overline{K}, where \overline{K} = \dfrac{h_{sec,o} - h_{sec,i}}{T_{sec,o}^{wb} - T_{sec,i}^{wb}} \end{cases} \tag{10}$$

When the IEC is activated in regions 2 and 4 (Fig. 3) in the dry mode, it operates as a heat exchanger. The process air exchanges heat from the exhaust air. When the air conditions are in regions 2 and 4, the process air is preheated by recovering heat from the exhaust air (secondary air). We determined the effectiveness of the heat exchanger using Equation (11) to predict the outlet temperature of the process air. In the dry mode, the sensible heat exchange effectiveness was calculated using the effectiveness-NTU model with the cross-flow heat exchanger, as shown in Equation (9). In winter, the proposed DOAS provides the minimum quantity of ventilation as a balanced flow; therefore, the efficiency was assumed to be 0.62 by designing the NTU and Cr as 2 and 1, respectively. In order to validate the precision of the IEC model, the simulated outlet air temperature was compared with the measured data; the results showed an error of 2.5% (Wet mode) and 1.9% (Dry mode), respectively, as shown in Appendix B.

$$\varepsilon_{IEC,dry} = \frac{\left|T_{pro,i} - T_{pro,o}\right|}{\left|T_{pro,i} - T_{sec,i}\right|} \tag{11}$$

3.2.3. Chiller

A cooling coil was used to cool the process air, maintain the target temperature in the DW-DOAS, and dehumidify the air, thereby satisfying the dehumidification load of the building in the CC-DOAS. The cooling capacity for the dry cooling operation was determined using the temperature difference (Equation (12)) and that for the wet cooling operation was determined using the enthalpy difference (Equation (13)). The target SA temperature, that is, the neutral temperature, in the DW-DOAS for the dry cooling operation was determined to be 24 °C, and the target air enthalpy in the CC-DOAS for the wet cooling operation was set to 10 °C for the saturated air state.

$$\dot{Q}_{req,cc,t} = \dot{m}_{SA} C_{p,a}\left(T_{cc,i} - T_{cc,tar}\right) \tag{12}$$

$$\dot{Q}_{req,cc,h} = \dot{m}_{SA}\left(h_{cc,i} - h_{cc,tar}\right) \tag{13}$$

To supply cold water to the cooling coil, we used an air-cooled chiller, whose model [41] was based on the performance curve in DOE2. The electric power of the chiller was indicated by the reference power and three performance curves (CAPFT, EIRFT, and EIRFPLR), as shown in Equations (14)–(18): The three performance curves, which were based on a polynomial equation, were determined using the OA temperature (T_{OA}) and supply cooling water temperature (T_{cws}). T_{cws} was set to 8 °C [42] for the cooling operations in the DW-DOAS and CC-DOAS.

$$P_{chiller} = P_{ref} \cdot CAPFT \cdot EIRFT \cdot EIRFPLR \tag{14}$$

$$CAPFT = 1.052729 + 0.037507 \cdot T_{cws} + 0.0002294 \cdot T_{cws}^2 - 0.003213844 \cdot T_{OA} - 0.0001016 \cdot T_{OA}^2 - 0.0005399 \cdot T_{cws} \cdot T_{OA} \tag{15}$$

$$EIRFT = 0.5363279857 - 0.0099693061 \cdot T_{cws} + 0.0004111273 \cdot T_{cws}^2 + 0.0041571647 \cdot T_{OA} + 0.0004088049 \cdot T_{OA}^2 - 0.0005399259 \cdot T_{cws} \cdot T_{OA} \tag{16}$$

$$EIRFPLR = 0.0354 + 0.7233 \cdot PLR + 0.2472 \cdot PLR^2 \tag{17}$$

$$PLR = \frac{\dot{Q}_{req,cc}}{\dot{Q}_{cap,chiller} \cdot CAPFT} \tag{18}$$

3.2.4. Desiccant wheel

The DW model was evaluated in a previous study using a prediction model for the RH and enthalpy of the outlet process air [43]. The model was based on the effectiveness of the inlet air of the process air and that of the secondary air (i.e., the exhaust air passing through the regeneration heater). To estimate the outlet temperature of the process air, we define the effectiveness models of the active DW using the inlet air conditions of the process air ($RH_{pro,i}$ and $h_{pro,i}$) and regeneration air ($h_{reg,i}$ and $RH_{reg,i}$), as shown in Equations (19) and (20).

$$\varepsilon_{RH,DW} = \frac{RH_{pro,i} - RH_{pro,o}}{RH_{pro,i} - RH_{reg,i}} \tag{19}$$

$$\varepsilon_{h,DW} = \frac{h_{pro,o} - h_{pro,i}}{h_{reg,i} - h_{pro,i}} \tag{20}$$

As shown in Equations (21) and (22), the RH and enthalpy effectiveness are driven by a series of equations using the independent variables of air velocity, air temperature, air humidity ratio, and rotational speed. The velocity of the process and regeneration air was set to 2 m/s as a balance flow in the DOAS, and the rotational speed of the DW was set to 20 rph [43]. The regeneration temperature for the DW-DOAS was set to 95 °C to satisfy the target humidity ratio (i.e., 7.63 g/kg) under the design conditions [44].

$$\varepsilon_{\mathrm{RH}} = \alpha_{vel,pro}\alpha_{vel,reg}\alpha_T\alpha_w\alpha_N \tag{21}$$

where

$$\alpha_{vel,pro} = 0.008343V_{pro,in}^2 - 0.04322V_{pro,in} + 0.16501,$$

$$\alpha_{vel,reg} = -0.003286V_{reg,in}^2 + 0.020519V_{reg,in} + 0.095525,$$

$$\alpha_T = 1.1903\ln\left(T_{reg,in} - T_{pro,in}\right) + 12.331,$$

$$\alpha_w = -4.519w_{pro,in} + 0.80627w_{reg,in} + 1,$$

$$\alpha_N = 0.0030464N + 4.2846$$

$$\varepsilon_h = \beta_{vel,pro}\beta_{vel,reg}\beta_T\beta_w\beta_N \tag{22}$$

where

$$\beta_{vel,pro} = 0.21763\left(V_{pro,in}\right)^{-0.66335},$$

$$\beta_{vel,reg} = 0.22113\left(V_{reg,in}\right)^{0.23493},$$

$$\beta_T = 0.0016778T_{reg,in} - 0.0056224T_{pro,in} + 1.671,$$

$$\beta_w = -44.505w_{reg,in} + 27.728w_{pro,in} + 1,$$

$$\beta_N = 0.13883N + 4.6438$$

3.3. Other components

3.3.1. Heat exchanger: sensible heat and enthalpy exchangers

The heat exchange systems used in the DW-DOAS and CC-DOAS are heat and enthalpy exchangers, respectively. The sensible heat exchanger in the DW-DOAS is used to precool the process air during cooling or to recover heat from the exhaust air during heating. The effectiveness of the heat exchanger is used to estimate the outlet air temperature passing through it. The sensible heat exchanger in the DW-DOAS operates similarly to the dry operation of the IEC in the proposed DOAS, and the heat exchanger effectiveness for predicting the outlet temperature is used, as shown in Equation (9).

The enthalpy exchanger used in the CC-DOAS operates to recover heat and moisture from the exhaust air stream to the SA stream. The sensible and latent effectiveness values were used to estimate the outlet air conditions of the enthalpy exchanger, as shown in Equations (23) and (24), respectively. The sensible effectiveness (ε_{sen}) and latent effectiveness (ε_{lat}) were assumed to be 0.6 and 0.5, respectively [45].

$$\varepsilon_{sen} = \frac{T_{pro,i} - T_{pro,o}}{T_{pro,i} - T_{sec,i}} \tag{23}$$

$$\varepsilon_{lat} = \frac{w_{pro,i} - w_{pro,o}}{w_{pro,i} - w_{sec,i}} \tag{24}$$

3.3.2. Electric heater

In this study, an electric heating coil was used to maintain the neutral temperature of the DOASs, and a regeneration heater was used to maintain the dehumidification performance of the DW. The power of the electric heater was assumed to be 100% [46] and the required heat capacity for heating was equal to the power of the electric heater.

Although the studied DOASs cannot satisfy the target temperature in winter or reclaim heat from the exhaust air, an electric heater can be used to heat the process air to a neutral temperature. The heating capacity for the heating season was determined using Equation (25). In the DW-DOAS, the regeneration heater was set to the target regeneration temperature (95 °C) to remove the latent load under the design conditions. As shown in Equation (26), the heating capacity of the regeneration heater was determined using the target regeneration and inlet air temperatures of the regeneration heating coil, which was the exhaust air temperature passing through

the heat exchanger.

$$\dot{Q}_{hc} = \dot{m}_a c_{p,a} \left(T_{SA} - T_{hc,i}\right) \tag{25}$$

$$\dot{Q}_{hc,reg} = \dot{m}_a c_{p,a} \left(T_{DW,reg} - T_{hc,reg,i}\right) \tag{26}$$

3.3.3. Fan and pump

As shown in Equations (27) and (28), the fans and pumps used in the studied DOASs were the constant-flow type, and their efficiencies (η_{fan} and η_{pump}) were assumed to be 60%. The pressure drops of the fan, which were set with reference to values from a previous study, are listed in Table 3. The head loss of the water pump used in the cooling coil for circulation and IEC for evaporation was assumed to be 15 m.

$$\mathrm{P_{fan}} = \frac{\dot{V}_a \Delta \mathrm{p}}{\eta_{fan}} \tag{27}$$

$$\mathrm{P_{pump}} = \frac{\dot{m}_{cws} \mathrm{g} \Delta h}{\eta_{pump}} \tag{28}$$

4. Simulation results

4.1. System operation loads of the DOASs

Fig. 9 shows the system loads of the DOASs for each component for an annual operation. The proposed DOAS performs isothermal dehumidification using the ID and utilizes free cooling in the IEC, requiring a lower heat load than the DW-DOAS and CC-DOAS. The dehumidification load of the proposed DOAS, which operated only for latent cooling, was 652.0 kW for the ID, 68.9% lower than that of the regeneration heater in the DW-DOAS and 10.0% lower than that of the cooling coil that operated in the CC-DOAS wet-cooling coil. The DW-DOAS would require auxiliary cooling and the CC-DOAS would require reheating to satisfy the target temperature. However, the proposed system, which uses a thermally independent cooling method and an ID, can reduce the load because auxiliary cooling or heating loads are not required. The sensible cooling load required to satisfy the target temperature of the process air in the DOASs was 163.9 kWh for the IEC in the proposed DOAS, 312.4 kWh for dry cooling coil in the DW-DOAS, and 480.9 kWh for the reheating coil in the CC-DOAS; the proposed system had a 47.5% and 65.9% lower energy requirement than the DW-DOAS and CC-DOAS, respectively. The heating load in winter was 276.4 kWh in the proposed DOAS and DW-DOAS, and 442.3 kWh in the CC-DOAS, indicating the low efficiency of the sensible heat exchanger in the CC-DOAS enthalpy exchanger. The results indicated that the loads required to operate the proposed DOAS, DW-DOAS, and CC-DPAS were 1092.3, 2683.3, and 1646.7 kWh, respectively, and that the thermal load of the proposed DOAS was 59.3% and 33.7% lower than that of the DW-DOAS and CC-DOAS, respectively.

4.2. System COP and dehumidification COP

To evaluate the energy performance of the studied DOASs, we estimated the monthly average system COP (Equation (29)) of the DOASs, as shown in Fig. 10. The results indicated that the monthly average system COP ranged from 0.85 to 3.61 in the proposed system, from 0.53 to 3.61 for the DW-DOAS, and from 1.68 to 7.4 for the CC-DOAS. In winter, because dehumidification was not required, the DOASs operated to supply minimum ventilation at a neutral temperature through heat exchangers and heating coils. The system COP of the DOASs for the heating season was approximately 3.6, and it decreased when the temperature difference between the room and the OA decreased because the heat recovered by the heat exchangers decreased. In the intermediate season, the system COP of the proposed DOAS was up to 21.3 through free cooling by the IEC, whereas those of the DW-DOAS and CC-DOAS were 3.73 and 7.38, respectively. In summer (June to August), the average COP of the proposed DOAS was 0.80, whereas those of the DW-DOAS and CC-DOAS were 0.57 and 0.90, respectively; it was 1.40 times higher than the DW-DOAS and 0.89 times lower than CC-DOAS, respectively, although the proposed system uses free-cooling effect by the IEC. Consequently, the COPs of the studied DOASs were similar in the winter, but the COP of the ID system was low in the summer, although the proposed system performed IEC air cooling. Therefore, the proposed system has a significant COP deviation depending on whether the ID system is operated, and the system COP is lower than that of the CC-DOAS but higher than that of the DW-DOAS.

$$COP_{sys} = \frac{|\dot{m}_{sa}(h_{OA} - h_{SA})|}{\sum \dot{P}}, \text{where } \sum \dot{P} = \dot{P}_{fan} + \dot{P}_{pump} + \dot{P}_{vac} + \dot{P}_{chiller} + \dot{P}_{heater} \tag{29}$$

To evaluate the thermal and energy efficiency of the ID system, the sensible to latent heat ratio (SLHR) and dehumidification COP

Table 3
Pressure drop of each component.

Components	Pressure drop
Heating coil and cooling coil	100 Pa [47]
Heat exchangers	100 Pa [48]
Isothermal dehumidifier	125 Pa [49]
Desiccant wheel	150 Pa [50]

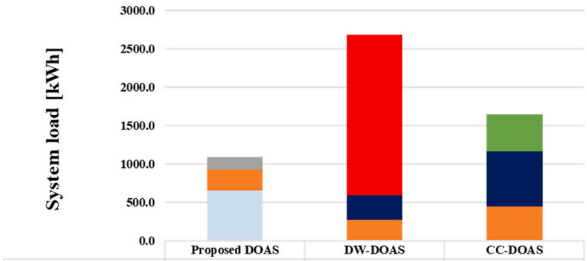

	Proposed DOAS	DW-DOAS	CC-DOAS
Reheat	0.0	0.0	480.9
Regeration	0.0	2094.5	0.0
Cooling coil	0.0	312.4	723.5
Indirect evaporative cooler	163.9	0	0
Heating coil	276.4	276.4	442.3
Isothermal dehumidifier	652.0	0.0	0.0

Fig. 9. System operation loads of the studied DOASs.

for each DOAS were defined and those performances were evaluated. The ratio of the sensible heat (i.e., the temperature change during dehumidification) to the latent cooling (i.e., the heat capacity of dehumidification) for satisfying the target humidity ratio of the SA was defined as the SLHR as given by Equation (30). A system that has a higher SLHR indicates that it has a high potential to have a lower thermodynamic efficiency for supplying neutral temperature in the dehumidification process. As shown in Fig. 11, the SLHR of the ID system was always zero because of its dehumidification process with isothermal; however, desiccant wheel (i.e., DW-DOAS) and cooling coil (i.e., CC-DOAS) has 8.09 and 1.32 in average, respectively. DW-DOAS and CC-DOAS require 20.2 °C of auxiliary cooling and 3.3 °C of reheating per 1g of water vapor dehumidification, respectively, showing that energy inefficiency occurs during the dehumidification operation process.

The COP of each system varied depending on the SA condition after the air passed the enthalpy exchanger as given by Equation (31). The average dehumidification COP of the proposed system was 1.34 and those of the DW-DOAS and CC-DOAS were 0.71 and 2.70, respectively. The dehumidification COP of the ID system is inferior to that of the CC-DOAS (i.e., the chiller), due to the low selectivity (50 in this study) of the membrane utilized in the ID system, resulting in an excessive load on the vacuum pump with a high compression ratio. Even with the thermodynamic benefit and free cooling operation, the low dehumidification COP of the ID system diminishes the system COP of the proposed DOAS.

$$SLHR = \frac{Sensible\ heat\ change}{Latent\ cooling} = \frac{C_p(T_i - T_o)}{h_{fg}(w_i - w_o)} \tag{30}$$

$$COP_{deh} = \frac{\left|\dot{m}_{sa} h_{fg}\left(w_{EX,o} - w_{SA}\right)\right|}{\sum \dot{P}}, \text{ where } \sum \dot{P} = \dot{P}_{vac} + \dot{P}_{chiller} + \dot{P}_{heater} \tag{31}$$

4.3. Annual energy consumption

Fig. 12 shows a comparison of the annual operational energy consumption of the studied DOASs. The proposed DOAS, DW-DOAS, and CC-DOAS consumed 3.52, 6.94, and 3.21 MWh of primary energy, respectively. Most of the annual energy was consumed by dehumidification, accounting for 74.1% (vacuum pump energy) in the proposed DOAS, 83.0% (regeneration heater) in the DW-DOAS, and 16.2% in the CC-DOAS (chiller). However, in the CC-DOAS, the energy consumed by the reheat coil to satisfy the target temperature (i.e., 24 °C in cooling) was 1.32 MWh, which offset the energy benefit of the chiller for dehumidification. Consequently, the proposed DOAS required 10.0% more energy than the CC-DOAS and reduced energy consumption by 49.3% compared with the DW-DOAS. In the case of the proposed system, chiller energy was saved by free cooling of IEC (0.28 MWh/year and 0.52 MWh/year compare with the CC-DOAS and the DW-DOAS). However, due to the low dehumidification COP of ID (0.78 in average), the proposed system required more energy than the CC-DOAS even though it required an overcooling and reheating of process air. In Section 5, we have discussed the relationship between the COP of the ID system and the total energy of the proposed DOAS.

Fig. 13 shows the monthly cumulative energy consumptions of the studied DOASs: from 59.0 to 920 kWh, 83.2 to 1600 kWh, and 114.5 to 550 kWh for the proposed DOAS, DW-DOAS, and CC-DOAS, respectively. The results indicated that the electric heater, in satisfying the target temperature (20 °C for heating), consumed less energy than in summer because the DOASs recovered heat from the exhaust of the RA using heat exchangers (sensible heat exchanger and enthalpy exchanger). In the studied DOASs, the cooling season (June to September) had a higher energy consumption than the other seasons (i.e., the intermediate season and winter); more latent cooling by the DOASs consumed more energy. Thus, the proposed DOAS can save energy through free cooling using the IEC in the intermediate season. However, in summer (hot and humid), it consumes more energy because of the low COP of the ID system for dehumidification.

5. Discussion: energy efficiency improvement via ID design

In the proposed system, most of the energy is consumed by the vacuum pump for dehumidification. This section analyzes the correlation between the COP of the ID and the energy consumed in the entire DOAS and the influencing factors that can increase the

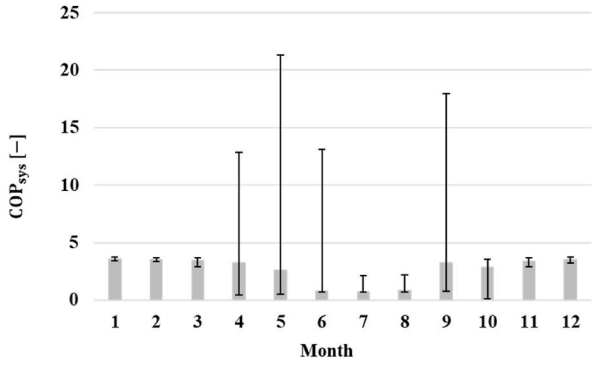

(a) Proposed DOAS

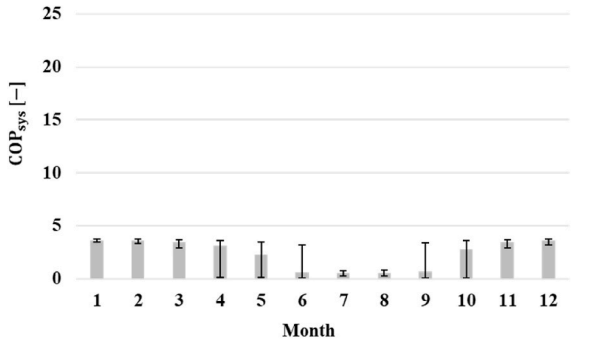

(b) DW-DOAS

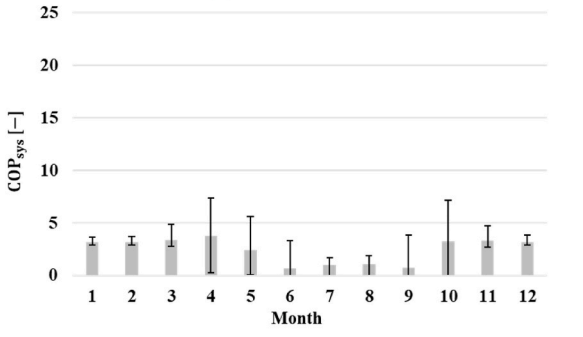

(c) CC-DOAS

Fig. 10. System COP of the studied DOASs (a) Proposed DOAS (b) DW-DOAS (c) CC-DOAS.

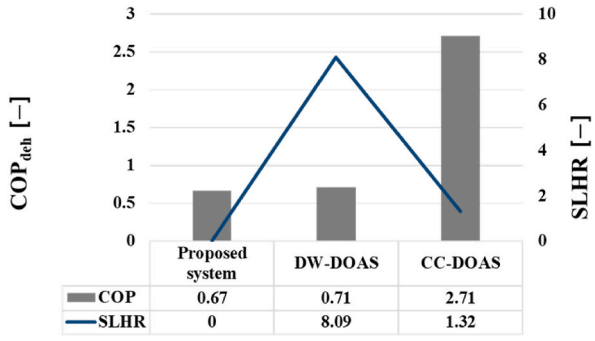

Fig. 11. Dehumidification performance of the studied DOASs in cooling operation.

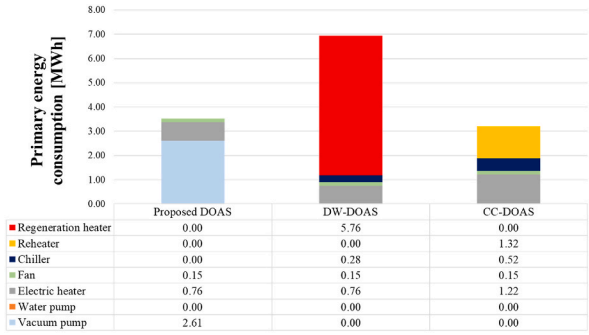

	Proposed DOAS	DW-DOAS	CC-DOAS
Regeneration heater	0.00	5.76	0.00
Reheater	0.00	0.00	1.32
Chiller	0.00	0.28	0.52
Fan	0.15	0.15	0.15
Electric heater	0.76	0.76	1.22
Water pump	0.00	0.00	0.00
Vacuum pump	2.61	0.00	0.00

Fig. 12. Annual energy consumptions of the studied DOASs.

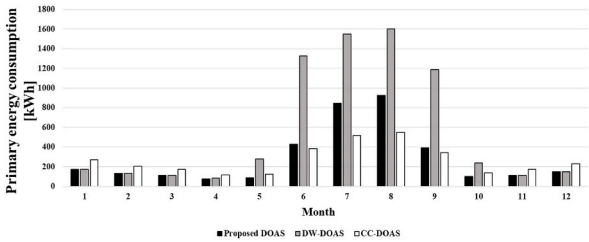

Fig. 13. Monthly energy consumption of the studied DOASs.

COP.

To improve the system COP of the ID-IECDOAS, its ID system must be increased for energy savings. The energy-saving potentials compared with the studied DOASs were evaluated by increasing the COP of the ID system. As the COP of the ID increased, the energy consumed for dehumidification decreased, resulting in a decrease in the annual energy consumption. The energy savings represent the percentage of energy consumed annually by each system, as shown in Equation (32). Fig. 14 shows the COP of the ID system, the annual energy savings of the proposed system, and the break-even points for the CC-DOAS. When the average COP of the ID system reached 0.78, which was 16.4% higher than that in this study, the energy consumption of the proposed system and the CC-DOAS reached the break-even point, and a 54% energy-saving effect compared with Reference B was achieved. If the COP of the ID system reaches 1, an energy-saving effect of 16.2% compared with the proposed system and the CC-DOAS is achieved, and an energy-saving effect of 61.5% compared with the DW-DOAS is achieved.

$$ESP_x = \frac{\sum \dot{P}_{proposed} - \sum \dot{P}_x}{\sum \dot{P}_x}, \text{where} x = \text{DW} - \text{DOAS or CC} - \text{DOAS} \tag{32}$$

To improve the energy performance of the ID system, we performed a parametric analysis for the COP with independent design parameters (membrane and vacuum pump characteristics) at the design condition, which is TAC 2.5 in Seoul, Korea (33.2 °C and 50.3% RH). In the base scenario, the independent parameters of the ID system were set to a selectivity of 50, permeance of 680 GPU, compression ratio of 101.3 (at a vacuum pressure of 1 kPa), and isentropic efficiency of 0.5. The operating parameters are listed in Table 4. The minimum and maximum values of selectivity were set to 62.5 and 32000 for dense membranes [51,52], and those of the permeance were 300 and 19200 GPU, respectively, based on previous studies. The ranges of the compression ratio and isentropic efficiency were 1.59–101.3 and 0.3–1, respectively. Parameter analysis was performed while sequentially changing each parameter within the operating range for each scenario and fixing the other parameters as the base scenario.

Fig. 15 depicts the sensitivities of each independent parameter to the COP of the ID system. When the selectivity increased from 62.5 to 32000, the system COP increased from 0.48 to 1.23. At a selectivity below 1000, the system COP increased rapidly but became nearly saturated at 1.23. As the selectivity increases, the gas load and energy consumption of the vacuum pump decrease because the amount of dry air permeated through the membrane decreases. When the permanence increased from 300 to 153600 GPU, the COP did not change because the moisture permanence and dry air permeance increased. The perimeter of the membrane affected the size and

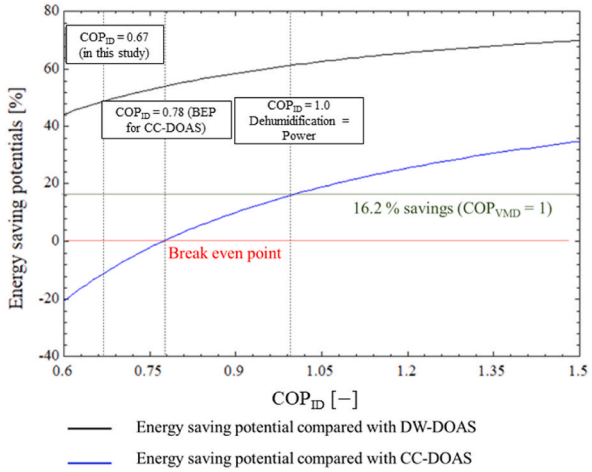

Fig. 14. Dehumidification COP of the ID-IECDOAS under various air conditions.

Table 4
Operation range for parametric analysis in the ID-IECDOAS.

Case	Selectivity [−]	Permeance [GPU]	Compression ratio [−]	Isentropic efficiency [−]
Base	50	680	101.3	0.5
(a)	25 to 32000	680	101.3	0.5
(b)	50	300 to 19200	101.3	0.5
(c)	50	680	1.59 to 101.3	0.5
(d)	50	680	101.3	0.3 to 1

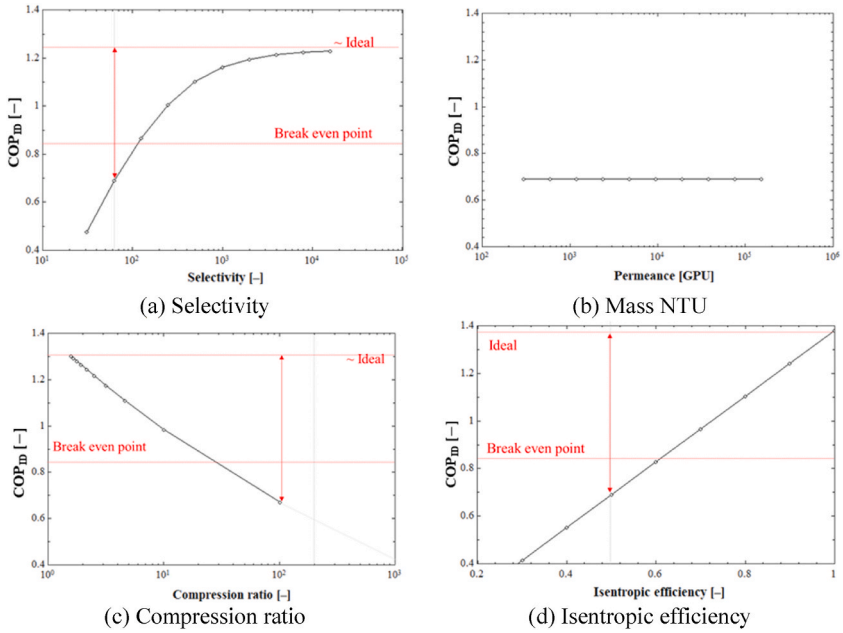

Fig. 15. Parametric analysis: COP improvement of the ID system (a) Selectivity (b) Mass NTU (c) Compression ratio (d) Isentropic efficiency.

capacity of the ID system but did not affect the COP. The operating parameters of the vacuum pump were compression ratio and isentropic efficiency as shown Equations (6) and (7). When the compression ratio increased from 1.5 to 101.3, the exhaust pressure of the vacuum pump decreased, the system COP decreased from 1.30 to 0.67. When the isentropic efficiency increased from 0.3 to 1, the system COP increased from 0.41 to 1.38.

Considering the ID system design for energy efficiency, the membrane selectivity should be greater than 1000 as a sensitive design parameter rather than the membrane permeance. The operation of the vacuum pump consumed the highest total power. The two parameters (compression ratio and isentropic efficiency) that directly affected the performance of the vacuum pump were most sensitive to the COP of the proposed system. Through the COP improvement of the ID system, the results showed that the proposed DOAS could sufficiently achieve the break-even point for energy saving.

6. Conclusion

In this paper, we propose a dedicated outdoor air system assisted by an isothermal dehumidifier and evaporative cooling (ID-IECDOAS) and evaluate its energy performance in comparison with conventional DOASs. The compared systems were a dedicated outdoor air system using a desiccant dehumidification system (DW-DOAS) and a condensation dehumidification system (CC-DOAS). To evaluate the energy performance of the proposed system, we investigated the energy consumption of the system COP and the thermal load of all the DOASs through detailed simulations using prediction models for each system component.

The results indicated that the total thermal load and average system COP of the proposed DOAS were 1092.3 kWh and 3.34, those of the DW-DOAS were 2683.3 kWh and 2.35, and those of the CC-DOAS were 1646.7 kWh and 2.43, respectively, because the proposed system uses an isothermal dehumidifier to independently deal with the sensible and latent cooling to reduce the thermal load. However, because of the low COP of the ID system, the energy consumption of the proposed system was higher than that of the CC-DOAS, although the free cooling of the IEC was used. Consequently, the total annual energy consumption of the proposed system was 10.0% higher than that of the CC-DOAS and 49.3% lower than that of the DW-DOAS.

To improve the energy performance of the proposed system, we conducted a parametric analysis of the energy performance of the ID system, which has the highest energy consumption in the proposed DOAS. The energy-saving potential of the proposed system was evaluated to estimate the effect of the COP of the ID system. When the COP of the ID system was greater than 0.78, the proposed DOAS had energy-saving potential compared with the reference DOAS (CC-DOAS). In addition, we conducted a parametric study on the COP of an ID system using four parameters (permeance, selectivity, compression ratio, and isentropic efficiency). The results showed that membrane selectivity and vacuum pump characteristics (compression ratio and isentropic efficiency) were closely related to the energy consumption of the COP of the ID system, and the influence of the independent parameters exceeded 0.78.

This study evaluated the applicability of the ID system in terms of its energy performance. However, additional investigation is required to determine its applicability from several viewpoints, including economic feasibility (i.e., cost analysis), indoor air quality (i.e., prevention of bio-contaminants), and control strategies to effectively manage the sensible and latent heat.

CRediT authorship contribution statement

Seong-Yong Cheon: Conceptualization, Methodology, Data curation, Writing – original draft. **Hye-Jin Cho:** Methodology, Validation. **Jae-Weon Jeong:** Supervision, Validation, Writing – review & editing.

Declaration of competing interest

The authors declare that they have no known competing financial interests or personal relationships that could have appeared to influence the work reported in this paper.

Data availability

Data will be made available on request.

Acknowledgment

This work was supported by the National Research Foundation of Korea (NRF) grants (No. 2022R1A2B5B02001975 and No. 2022R1A4A1026503).

Appendix A

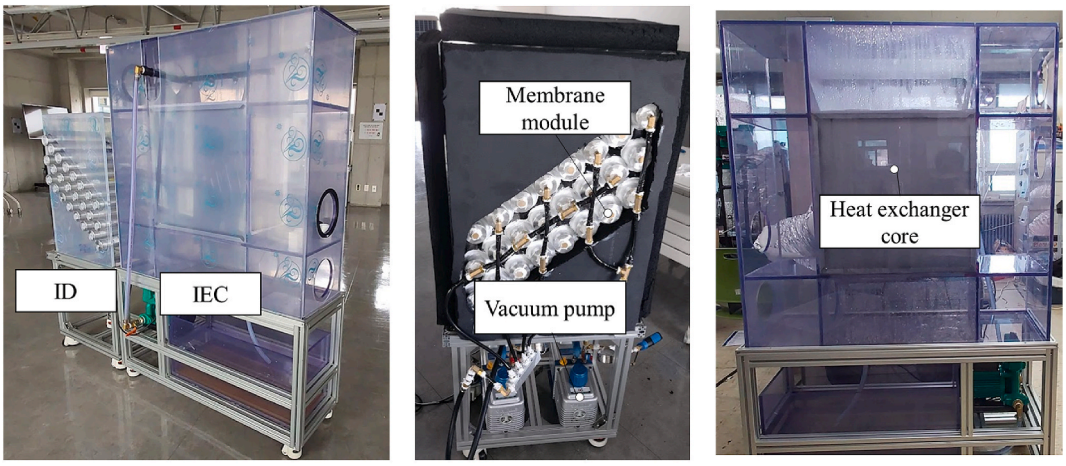

Fig. A.1. Experimental setup of the ID-IECDOAS (a) ID-IECDOAS (b) ID (c) IEC.

Appendix B

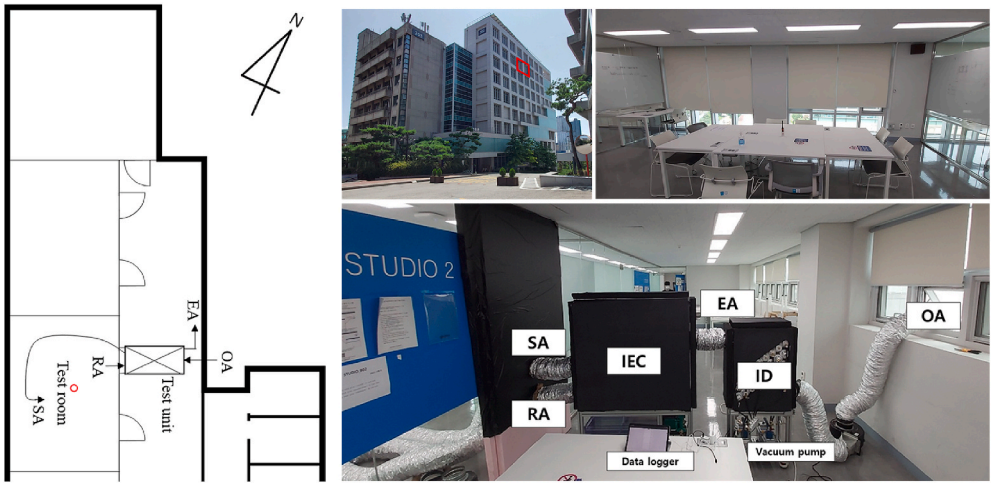

Fig. B.1. Experimental setup for simulation model validation of the proposed system.

Table B.1
Simulation model validation with experimental data

Contents	Inlet air	Simulation (outlet air)	Experiment (outlet air)	Error [%]
ID (Typical condition)	32 DBT and 13 g/kg	32 DBT and 10 g/kg	30 DBT and 10.5 g/kg	4.7
ID (Humid condition)	28 DBT and 17 g/kg	32 DBT and 11 g/kg	27 DBT and 12.5 g/kg	12
IEC: Wet mode	30 DBT and 10.5 g/kg	20 DBT and 10.5 g/kg	20.5 DBT and 10.5 g/kg	2.5
IEC: Dry mode	28 DBT and 11.2 g/kg	25.1 DBT and 11.2 g/kg	25.6 DBT and 11.2 g/kg	1.9

Conditions: The permeate side pressure is 3.3 kPa and the room air conditions are 24 DBT and 60% of relative humidity (Steady state condition over 10 min).

References

[1] IEA, 2013 webinar energy efficient building envelope technology road map, Available from: https://cleanenergysolutions.org/training/iea-s-energy-efficient-building-envelope-technology-roadmap. accessed Jul 20, 2023.
[2] DOE, Building America Research-To-Market Plan, United States Department of Energy, 2015.
[3] J. Munk, J. Winkler, Effect of occupant behavior on peak cooling and dehumidification loads in typical and high-efficiency homes, Energy Build. 184 (2019) 122–140. https://doi:10.1016/j.enbuild.2018.10.044.
[4] J. Murphy, Dehumidification performance of HVAC systems, ASHRAE J. 44 (2002) 23–31.

[5] A. Bakker, J.A. Siegel, M.J. Mendell, J. Peccia, Building and environmental factors that influence bacterial and fungal loading on air conditioning cooling coils, Indoor Air 28 (5) (2018) 689–696.
[6] Y. Wu, A. Chen, I. Luhung, E.T. Gall, Q. Cao, V.W. Chang, W.W. Nazaroff, Bioaerosol deposition on an air-conditioning cooling coil, Atmos. Environ. 144 (2016) 257–265.
[7] A. Gurubalan, M.P. Maiya, P.J. Geoghegan, A comprehensive review of liquid desiccant air conditioning system, Appl. Energy 254 (2019), 113673.
[8] M. Sultan, El-Sharkawy II, T. Miyazaki, B.B. Saha, S. Koyama, An overview of solid desiccant dehumidification and air conditioning systems, Renew. Sustain. Energy Rev. 46 (2015) 16–29.
[9] H. Ren, Z. Ma, W. Li, V.V. Tyagi, A.K. Pandey, Optimisation of a renewable cooling and heating system using an integer-based genetic algorithm, response surface method and life cycle analysis, Energy Convers. Manag. 230 (2021), 113797.
[10] C. Dong, R. Qi, L. Zhang, L. Lu, Performance enhancement of solar-assisted liquid desiccant dehumidifiers using super-hydrophilic surface, Energy Build. 199 (2019) 461–471.
[11] J.L. Niu, L.Z. Zhang, H.G. Zuo, Energy savings potential of chilled-ceiling combined with desiccant cooling in hot and humid climates, Energy Build. 34 (5) (2002) 487–495, https://doi.org/10.1016/S0378-7788(01)00132-3.
[12] M.H. Kim, J.Y. Park, M.K. Sung, A.S. Choi, J.W. Jeong, Annual operating energy savings of liquid desiccant and evaporative-cooling-assisted 100% outdoor air system, Energy Build. 76 (2014) 538–550, https://doi.org/10.1016/j.enbuild.2014.03.006.
[13] J. Woods, Membrane processes for heating, ventilation, and air conditioning, Renew. Sustain. Energy Rev. 33 (2014) 290–304. https://doi:10.1016/j.rser.2014.01.092.
[14] M. Qu, O. Abdelaziz, Z. Gao, H. Yin, Isothermal membrane-based air dehumidification: a comprehensive review, Renew. Sustain. Energy Rev. 82 (2018) 4060–4069. https://doi:10.1016/j.rser.2017.10.067.
[15] A.J. Fix, J.E. Braun, D.M. Warsinger, Vapor-selective active membrane energy exchanger for high efficiency outdoor air treatment, Appl. Energy 295 (2021), https://doi.org/10.1016/j.apenergy.2021.116950.
[16] M. Shehadi, Review of humidity control technologies in buildings, J. Build. Eng. 19 (2018) 539–551.
[17] R. Xing, Y. Rao, W. TeGrotenhuis, N. Canfield, F. Zheng, D.W. Winiarski, W. Liu, Advanced thin zeolite/metal flat sheet membrane for energy efficient air dehumidification and conditioning, Chem. Eng. Sci. 104 (2013) 596–609. https://doi:10.1016/j.ces.2013.08.061.
[18] S.J. Metz, W.J.C. Vandeven, J. Potreck, M.H.V. Mulder, M. Wessling, Transport of water vapor and inert gas mixtures through highly selective and highly permeable polymer membranes, J. Membr. Sci. 251 (1–2) (2005) 29–41. https://doi:10.1016/j.memsci.2004.08.036.
[19] T.D. Bui, F. Chen, A. Nida, K.J. Chua, K.C. Ng, Experimental and modeling analysis of membrane-based air dehumidification, Sep. Purif. Technol. 144 (2015) 114–122. https://doi:10.1016/j.seppur.2015.02.019.
[20] T.D. Bui, Y. Wong, M.R. Islam, K.J. Chua, On the theoretical and experimental energy efficiency analyses of a vacuum-based dehumidification membrane, J. Membr. Sci. 539 (2017) 76–87. https://doi:10.1016/j.memsci.2017.05.067.
[21] P. Scovazzo, A.J. Scovazzo, Isothermal dehumidification or gas drying using vacuum sweep dehumidification, Appl. Therm. Eng. 50 (1) (2013) 225–233. https://doi:10.1016/j.applthermaleng.2012.05.019.
[22] P. Scovazzo, R. MacNeill, Membrane module design, construction, and testing for vacuum sweep dehumidification (VSD): Part I, prototype development and module design, J. Membr. Sci. 576 (2019) 96–107. https://doi:10.1016/j.memsci.2018.12.076.
[23] D.E. Claridge, C. Culp, W. Liu, M. Pate, J. Haberl, J. Bynum, O. Tanskyi, F. Schaff, A new approach for drying moist air: the ideal Claridge-Culp-Liu dehumidification process with membrane separation, vacuum compression and sub-atmospheric condensation, Int. J. Refrig. 101 (2019) 211–217. https://doi:10.1016/j.ijrefrig.2019.03.025.
[24] ASHRAE 62.1-2016. Ventilation for Acceptable Indoor Air Quality. (Atlanta).
[25] S.A. Klein, W.A. Beckman, J.W. Mitchell, J.A. Duffie, N.A. Duffie, T.L. Freeman, et al., TRNSYS 16-A, Transient System Simulation Program, University of Wisconsin, Madison, WI, 2004. Available from: http://sel.me.wisc.edu/trnsys/.
[26] K.E. Agency, Regulations for the Operation of Building Energy Efficiency Rating System, 2016.
[27] B.C. Kwag, S. Han, G.T. Kim, B. Kim, J.Y. Kim, Analysis of the effects of strengthening building energy policy on multifamily residential buildings in South Korea, Sustainability 12 (9) (2020). https://doi:10.3390/SU12093566.
[28] ASHRAE standard 55, Thermal Environmental Conditions for Human Occupancy, 2017. Atlanta.
[29] ASHRAE standard 90.1-2016, Energy Standard for Buildings except Low-Rise Residential Buildings, 2016. Atlanta.
[30] S.Y. Cheon, S.J. Lee, L.W. Lin, J.W. Jeong, Experimental Study on Dehumidification Performance of a Vacuum-Based Membrane Dehumidifier ASHRAE Virtual Annual Conference; June 28, 2021, 2021.
[31] S.Y. Cheon, H.J. Cho, J.W. Jeong, Simplified effectiveness-NTU model for a vacuum membrane dehumidifier applied to air conditioning, Appl. Therm. Eng. 210 (2022), 118404.
[32] B. Belaissaoui, Y. Le Moullec, H. Hagi, E. Favre, Energy efficiency of oxygen enriched air production technologies: cryogeny vs membranes, Sep. Purif. Technol. 125 (2014) 142–150. https://doi:10.1016/j.seppur.2014.01.043.
[33] C.P. Kothandaraman, S. Subramanyan, Heat and Mass Transfer Data, sixth ed., New Age International Publishers, New Delhi, 2007.
[34] L.Z. Zhang, S.M. Huang, Coupled heat and mass transfer in a counter flow hollow fiber membrane module for air humidification, Int. J. Heat Mass. Int. J. Heat Mass Trans. 54 (5–6) (2011) 1055–1063. https://doi:10.1016/j.ijheatmasstransfer.2010.11.025.
[35] B. Yang, W. Yuan, F. Gao, B. Guo, A review of membrane-based air dehumidification, Indoor Built Environ. 24 (1) (2015) 11–26. https://doi:10.1177/1420326X13500294.
[36] S.Y. Cheon, H.J. Cho, J.W. Jeong, Experimental study of vacuum-based membrane dehumidifier for HVAC system: parametric analysis and dehumidification performance, Energy Convers. Manag. 270 (2022), 116252.
[37] R.H. Mohammed, M. El-Morsi, O. Abdelaziz, Indirect evaporative cooling for buildings: a comprehensive patents review, J. Build. Eng. 50 (2022), 104158.
[38] Ala Hasan, Going below the wet-bulb temperature by indirect evaporative cooling: analysis using a modified ε-NTU method, Appl. Energy 89 (1) (2012) 237–245.
[39] Z. Liu, A. William, M. Mark, Simplified thermal modeling of indirect evaporative heat exchangers, HVAC R Res. 19 (3) (2013) 257–267.
[40] M.H. Kim, D.S. Jeong, J.W. Jeong, Practical thermal performance correlations for a wet-coil indirect evaporative cooler, Energy Build. 96 (2015) 285–298.
[41] M. Hydeman, N. Webb, P. Sreedharan, S. Blanc, Development and testing of a reformulated regression-based electric chiller model, ASHRAE Trans. 108 (2) (2002) 1118–1127.
[42] H. Lim, J.W. Jeong, Energy saving potential of thermoelectric radiant cooling panels with a dedicated outdoor air system, Energy Build. 169 (2018) 353–365. https://doi:10.1016/j.enbuild.2018.03.062.
[43] S. De Antonellis, M. Intini, C.M. Joppolo, Desiccant wheels effectiveness parameters: correlations based on experimental data, Energy Build. 103 (2015) 296–306. https://doi:10.1016/j.enbuild.2015.06.041.
[44] M.H. Ahmed, N.M. Kattab, M. Fouad, Evaluation and optimization of solar desiccant wheel performance, Renew. Energy 30 (3) (2005) 305–325. https://doi:10.1016/j.renene.2004.04.010.
[45] Y. Choi, D. Song, D. Seo, J. Kim, Analysis of the variable heat exchange efficiency of heat recovery ventilators and the associated heating energy demand, Energy Build. 172 (2018) 152–158. https://doi:10.1016/j.enbuild.2018.04.066.
[46] L.M. Ayompe, A. Duffy, M. Mc Keever, M. Conlon, S.J. McCormack, Comparative field performance study of flat plate and heat pipe evacuated tube collectors (ETCs) for domestic water heating systems in a temperate climate, Energy 36 (5) (2011) 3370–3378. https://doi:10.1016.
[47] P. Raftery, M. Keane, A. Costa, Calibrating whole building energy models: detailed case study using hourly measured data, Energy Build. 43 (12) (2011) 3666–3679. https://doi:10.1016/j.enbuild.2011.09.039.
[48] M.H. Kim, D.S. Yoon, H.J. Kim, J.W. Jeong, Retrofit of a liquid desiccant and evaporative cooling-assisted 100% outdoor air system for enhancing energy saving potential, Appl. Therm. Eng. 96 (2016) 441–453. https://doi:10.1016/j.applthermaleng.2015.11.088.

[49] A.A. Bukshaisha, B.M. Fronk, Investigation of Seasonal Performance of a Membrane Heat Pump System in Different Climate Regions, Oregon State University MS thesis, 2018.
[50] Available from:, NovelAire technologies, Inc., 2021 https://www.novelaire.com/. accessed Jul 20 2023.
[51] S.J. Metz, W.J.C. Van de Ven, J. Potreck, M.H.V. Mulder, M. Wessling, Transport of water vapor and inert gas mixtures through highly selective and highly permeable polymer membranes, J. Membr. Sci. 251 (1–2) (2005) 29–41.
[52] F.H. Akhtar, M. Kumar, K.V. Peinemann, Pebax® 1657/Graphene oxide composite membranes for improved water vapor separation, J. Membr. Sci. 252 (2017) 187–194.